Phase transition of a triangular lattice Ising antiferromagnet FeI_2

K. Katsumata,[1] H. Aruga Katori,[2] S. Kimura,[3] Y. Narumi,[4] M. Hagiwara,[3] and K. Kindo[5]
[1]*RIKEN SPring-8 Center, Harima Institute, Sayo, Hyogo 679-5148, Japan*
[2]*RIKEN, Hirosawa 2-1, Wako, Saitama 351-0198, Japan*
[3]*KYOKUGEN, Osaka University, Toyonaka, Osaka 560-8531, Japan*
[4]*Institute for Material Research, Tohoku University, Sendai, Miyagi 980-8577, Japan*
[5]*ISSP, University of Tokyo, Kashiwa, Chiba 277-8581, Japan*

(Received 25 April 2010; revised manuscript received 18 June 2010; published 2 September 2010)

The phase transition of FeI_2 is revisited. This material has the hexagonal crystal structure and shows an antiferromagnetic order at $T_N = 9.3$ K in zero field. When an external magnetic field is applied along the *c* axis below T_N, successive metamagnetic transitions occur. The magnetism of FeI_2 has been interpreted based on the further neighbor interaction model on the triangular net. However, the exchange interaction constants derived from the analysis do not seem realistic. We have measured the magnetic susceptibility, magnetization, and specific heat on single crystals of FeI_2. From the specific-heat measurement, the temperature versus magnetic field phase diagram is constructed, in which five distinct magnetic phases, namely, the antiferromagnetic and four ferrimagnetic ones, exist. The magnetization measurement reveals that magnetization steps appear at $\frac{1}{3}$, $\frac{12}{25}$, $\frac{13}{25}$ and between $\frac{16}{25}$ and $\frac{17}{25}$ of the saturation magnetization, $M_s = 3.5$ μ_B/Fe. Based on an experimental evidence, we argue that a lattice distortion occurs below T_N and the exchange interaction between spins on a triangle becomes anisotropic. We discuss the phase transition using the anisotropic triangular lattice model with J_1, J_2, and J_3. From the analysis of the metamagnetic transition fields, we obtain, $2.5 < J_1/k_B < 3.0$ K, $-16.2 < J_2/k_B < -15.2$ K, and $-16.4 < J_3/k_B < -14.4$ K.

DOI: 10.1103/PhysRevB.82.104402 PACS number(s): 75.30.Kz, 75.60.Ej, 75.80.+q, 75.40.Cx

I. INTRODUCTION

The phase transition of an antiferromagnetic triangular lattice (ATL) has attracted much attention since the pioneering work by Wannier,[1] who showed rigorously that an Ising model ATL does not show any long-range order down to zero Kelvin. Physically, this originates from the geometric frustration by which all the neighboring spins on the triangles cannot align antiparallel to each other at the same time. The ground state is composed of two spins of one kind and one of another in each triangle.[2] When a magnetic field is applied, a spin arrangement ↑↑↓ is realized giving rise to a magnetization with one third of the saturation magnetization, M_s. This $M_s/3$ plateau persists up to the saturation field.[3]

In real materials, the exchange interaction paths in the triangular net are generally more complex, for which an anisotropic triangular lattice, or a further neighbor interaction models shown in Figs. 1(a) and 1(b), respectively, may be applicable. Stephenson[4] showed rigorously that a long-range magnetic order occurs at a finite temperature even in an Ising ATL, when all the interactions in the anisotropic triangular lattice model [Fig. 1(a)] are antiferromagnetic and $|J_1| > |J_2| > |J_3|$. The magnetic structure in the ordered state of this model is given in Fig. 1(c). The ground-state property and phase transition of an Ising model on the triangular net with further neighbor interactions [Fig. 1(b)] were studied by several authors.[5–8]

In this paper, we study the phase transition of the hexagonal Ising antiferromagnet FeI_2. The magnetic properties of MX_2 compound have been studied for many years,[9] where, *M* and *X* stand for 3*d* transition metal and halogen ions, respectively. The FeX_2 compound shows an antiferromagnetic order at low temperatures. The magnetic structure in the ordered state of $FeCl_2$ and $FeBr_2$ is the one in which the spins within a metal layer form ferromagnetic (F) sheets and the spins in adjacent layers are antiparallel.[10] On the other hand, in the magnetic structure of FeI_2, spins within a metal layer form antiferromagnetic sheets.[11] This indicates that the exchange interaction within a layer changes from ferromagnetic to antiferromagnetic with the change in the halogen ions. The origin of this change in the exchange interaction has not been discussed in an atomic level of detail.

The magnetic ordering in FeI_2 has been discussed in terms of the further neighbor interaction model.[12] From an analysis of the experimental results, the exchange interaction constant between planes about three times larger than that within the plane has been obtained.[12] One would expect that the intra-

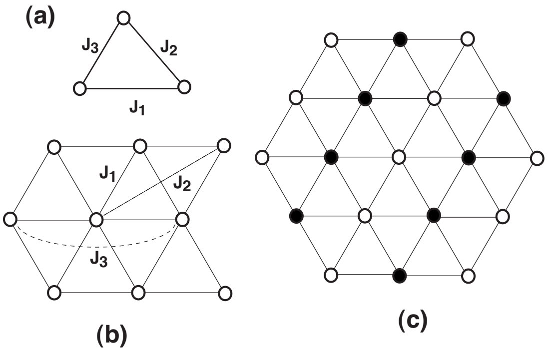

FIG. 1. (a) An anisotropic triangular lattice model. (b) The first-, second-, and third-nearest-neighbor exchange interaction model of a triangular net. (c) The magnetic structure of an Ising model on the anisotropic triangular lattice [Fig. 1(a)] predicted to appear when all the interactions are antiferromagnetic and $|J_1| > |J_2| > |J_3|$. Open and filled circles show up and down spins, respectively.

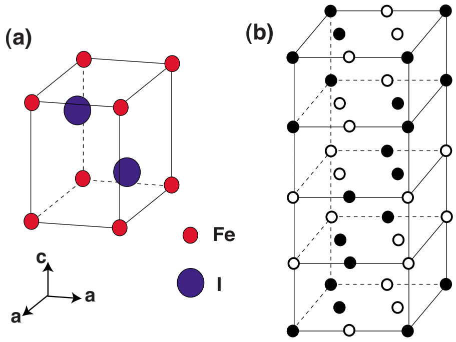

FIG. 2. (Color online) (a) The crystal structure of FeI_2. (b) The magnetic structure of FeI_2 in zero field. Open and filled circles show the magnetic moments pointing parallel or antiparallel to the *c* axis, respectively.

layer interaction is much stronger than the interlayer one as in $FeCl_2$.[12]

When a magnetic field is applied along the spin easy axis which is the *c* axis of the crystal, $FeCl_2$ and $FeBr_2$ show a first-order transition from the antiferromagnetic to ferromagnetic state at low temperatures.[9] A more complex magnetization process has been observed in FeI_2, where at least four magnetization changes are seen.[13,14] The magnetization process was discussed based on the further neighbor interaction model.[14] From an analysis of the experimental results, the third-nearest-neighbor interaction constant with almost the same magnitude as the nearest-neighbor one has been obtained.[14] This result does not appear to be realistic because the exchange interaction in an insulating material decays rapidly with the distance between magnetic ions.

In this paper, we try to understand the enigmatic properties of FeI_2 from the measurements of magnetic susceptibility, magnetization, and specific heat. We discuss, first, the electronic state of Fe^{2+} in FeI_2 and the exchange interaction to justify that the material can be modeled by an Ising antiferromagnet. Then, the experimental results are interpreted based on the anisotropic triangular lattice model.

II. CRYSTAL AND MAGNETIC STRUCTURE

The compound FeI_2 has the hexagonal (trigonal) crystal structure (space group $P\bar{3}m1$) shown in Fig. 2(a). The lattice constants are, $a=4.03$ Å and $c=6.75$ Å.[11] This material exhibits an antiferromagnetic order at $T_N=9.3$ K.[12] The magnetic structure in zero field of FeI_2 determined from the neutron-diffraction experiment[11] is shown in Fig. 2(b).

When an external magnetic field, B, is applied along the *c* axis, FeI_2 shows successive magnetic phase transitions. The magnetic field versus temperature phase diagram determined from the magnetization and neutron-diffraction measurements[14] is shown schematically in Fig. 3(a). Figure 3(b) shows the magnetic structure determined from the neutron-diffraction study at temperature, $T=1.4$ K and $B=5.5$ T corresponding to phase F1.[14] In this phase, the wave vectors, $\boldsymbol{k_1}=[\frac{1}{6}\frac{1}{6}0]$, $\boldsymbol{k_2}=[\frac{1}{3}\overline{\frac{1}{6}}0]$, and $\boldsymbol{k_3}=[\frac{1}{6}\overline{\frac{1}{3}}0]$ are observed.[14] The magnetic structure determined at $T=1.4$ K and $B=7.1$ T corresponding to phase F2 is shown in Fig. 3(c). In this phase, the wave vectors, $\boldsymbol{k_1}=[\frac{1}{5}\frac{1}{5}0]$, $\boldsymbol{k_2}=[\frac{2}{5}\overline{\frac{1}{5}}0]$, and $\boldsymbol{k_3}=[\frac{1}{5}\overline{\frac{2}{5}}0]$ are observed.[14] Wiedenmann *et al.*[14] have not observed any magnetic long-range order in phase F3 and suggested that it was an amorphous or floating phase. The magnetic structure of phase F4 does not seem to be determined completely. Wiedenmann *et al.*[14] presented the magnetic structure shown in Fig. 3(d) defined by the single wave vector, $\boldsymbol{k_3}=[\frac{1}{5}\overline{\frac{2}{5}}0]$. In phases F1, F2, and F4 the magnetic sheet shown in Figs. 3(b)–3(d), respectively, is stacked along the *c* axis and the spins in adjacent layers are parallel.

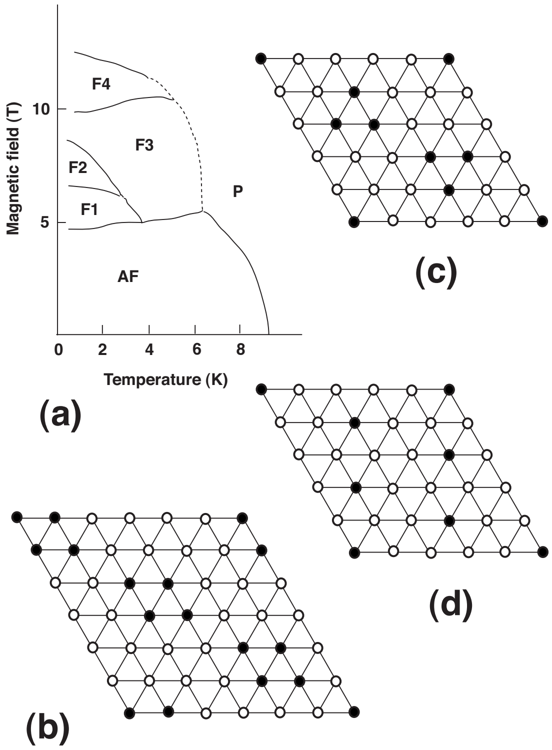

FIG. 3. (a) The magnetic field versus temperature phase diagram of FeI_2. Here, only the phase boundary curves in Ref. 14 are reproduced. (b) The magnetic structure in the *c* plane of phase F1. (c) The magnetic structure in the *c* plane of phase F2. (d) The magnetic structure in the *c* plane of phase F4. Open and filled circles show the magnetic moments pointing parallel or antiparallel to the field direction, respectively.

III. EXPERIMENTAL DETAILS

Polycrystalline samples of FeI_2 were prepared by a direct reaction of iron (Johnson Matthey, 99.999%) with iodine in an evacuated silica tube. Single crystals of FeI_2 were grown by the Bridgman method.

Magnetization, M, measurements under steady fields were done with a MagLab$^{\mathrm{VSM}}$ vibrating-sample magnetometer (Oxford Instruments, U.K.). The temperature and magnetic field ranges available with this magnetometer are, $1.5 \leq T \leq 300$ K and $0 \leq B \leq 12$ T. The magnetization measurement up to 50 T was conducted at KYOKUGEN, Osaka University with a pulsed field magnet.

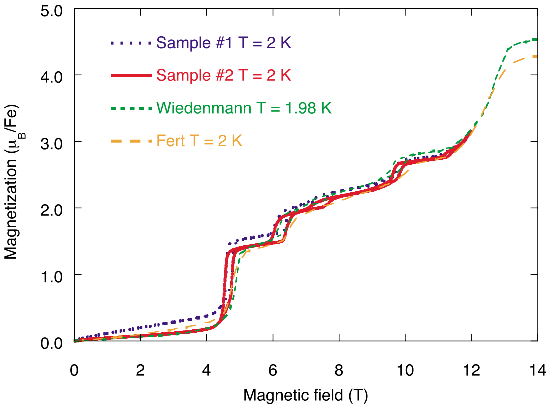

FIG. 4. (Color online) The magnetic field dependence of magnetization in FeI_2 measured at 2 K for the two crystals cut from different boules (red and blue). The external magnetic field is applied along the c axis of the crystals. Also shown is the magnetization curve reported by Fert *et al.* (Ref. 13) (orange) and Wiedenmann *et al.* (Ref. 14) (green).

Specific heat, C_p, measurements were performed with a MagLab^{HC} microcalorimeter (Oxford Instruments, U.K.). This microcalorimeter employs a thermal relaxation method. The measurements were conducted in two modes, namely, the temperature and field scans. In the temperature scan, heat pulses were applied after stabilizing the temperature of the sample to a desired value, T_0 and decay of the sample temperature was measured, from which C_p was estimated. The value of T_0 was changed stepwise until the final temperature was reached. In the field scan, the magnetic field was set to a desired value B_0 and the same measurement as above was performed. The value of B_0 was changed stepwise under a fixed temperature until the final field was attained. In both of the temperature and field scans, two transient curves, corresponding to the rise and fall of the heat pulse, were recorded. By flipping over one curve and averaging it with the other, significant improvements are obtained. The temperature and magnetic field ranges accessible with this calorimeter are, $0.45 \leq T \leq 200$ K and $0 \leq B \leq 12$ T.

IV. RESULTS

A. Susceptibility

We measured the magnetic susceptibility parallel to the c axis (not shown) and obtained almost the same result as reported before.[12] Normally, the magnetic susceptibility, $\chi_{\parallel}$, parallel to the easy axis of a uniaxial antiferromagnet decreases with decreasing temperature below T_N, and becomes zero at $T=0$. However, we obtained a finite value $\chi_{\parallel}(T \to 0) \simeq 0.055$ (emu/mole), and a different value, $\chi_{\parallel}(T \to 0) \simeq 0.017$ (emu/mole) has been reported in a different sample.[12] In the next section we will discuss the origin of the finite value in $\chi_{\parallel}$ at low temperatures.

B. Magnetization

Figure 4 shows the magnetic field dependence of magnetization measured in a steady field up to 12 T for the two samples (samples #1 and 2) cut from different boules. We also plot the magnetization curves reported before.[13,14] All the magnetization curves show an initial slope that differs from sample to sample. The magnetization of the sample #1 is the largest up to ~6 T. However, all the magnetization curves are close to each other at $6.5 < B < 12$ T.

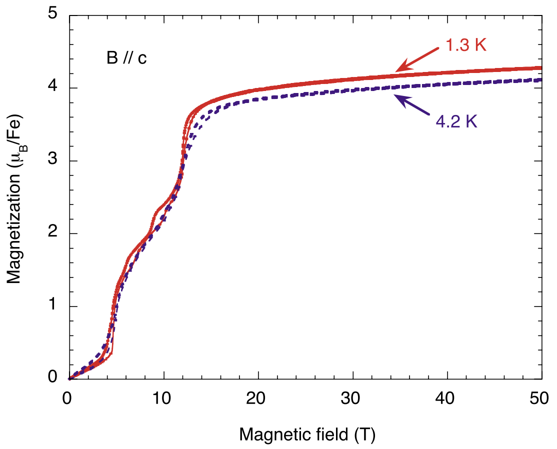

FIG. 5. (Color online) The magnetic field dependence of magnetization in FeI_2 measured in a pulsed field up to 50 T.

The experimental fact that the initial slope in the magnetization curve depends on samples suggests it comes from impurities or crystal imperfections. If it were due to paramagnetic impurities, one may use the Brillouin function to describe the magnetization coming from the impurities. The Brillouin function at $T=2$ K becomes practically saturated above 4 T for both of Fe^{2+} (spin, $S=2$ and g value, $g=2$) and Fe^{3+} ($S=\frac{5}{2}$ and $g=2$) ions. The saturated part of the magnetization due to the paramagnetic impurities would give a constant term, which is sample dependent, to the magnetization at high fields, in contradiction with the observation explained above. Therefore, we may discard the possibility of paramagnetic impurities to describe the initial slope. As will be discussed later, a lattice distortion probably occurs below T_N to relieve partially the magnetic frustration. Depending on the crystal growth conditions, the imperfections in the crystal may differ from sample to sample. The spins contained in the imperfections may behave differently from those in the bulk and will cause the sample-dependent initial slope in the magnetization curve.

In order to determine the value of saturation magnetization of FeI_2, we measured the magnetization up to 50 T at $T=1.3$ and 4.2 K. The result is shown in Fig. 5. Contrary to our expectation, the magnetization does not saturate. Instead, it increases steadily with increasing field.

As is seen in Fig. 5, the magnetization measured at $T=1.3$ K shows a steep increase at $\simeq 12$ T and becomes less field dependent above this field. We call the phase above this field a saturated F one, although the magnetization is not fully saturated. The hysteresis associated with this transition disappears at $\simeq 15$ T, where the saturation magnetization, M_s, is $\simeq 3.8$ μ_B/Fe. This value of $M_s (=g \cdot \sigma)$ is consistent with the g value of 3.5 determined from the electron spin resonance (ESR) measurements[15,16] and $\sigma=1$ (the ground state of FeI_2 will be discussed later). Gelard *et al.*[11] obtained

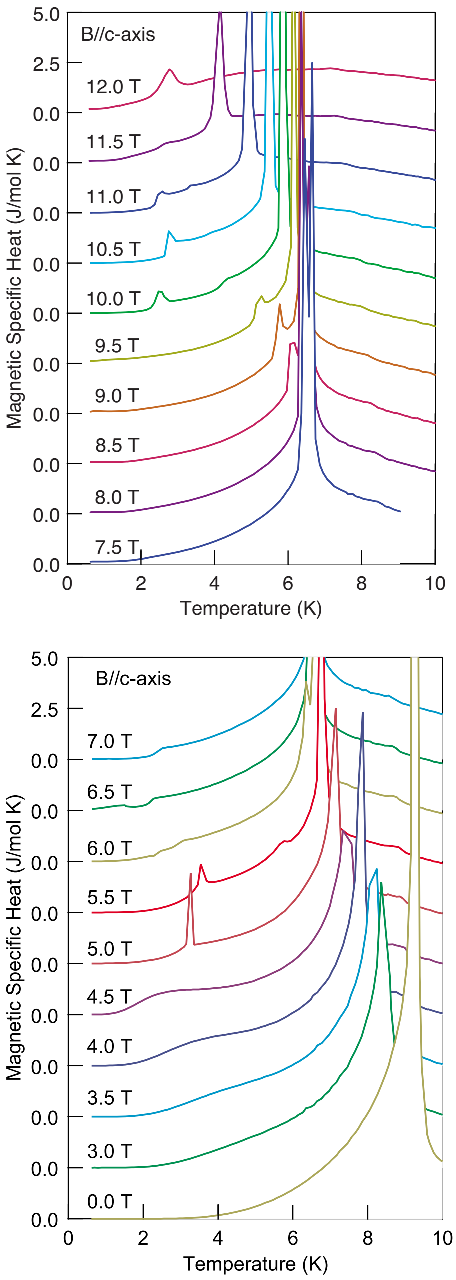

FIG. 6. (Color online) The temperature dependence of magnetic specific heat in FeI_2 measured in zero and nonzero applied magnetic fields. The scale for the ordinate is given to the uppermost curve and the base line for the remaining curves is shifted downwards by 2.5 J/mol K each.

the value, 3.7 μ_B for the magnetic moment of Fe in FeI_2 from the neutron-diffraction study.

C. Specific heat

The temperature dependence of magnetic specific heat, C_m, obtained from the temperature scan is shown in Fig. 6. The lattice specific heat was subtracted from the measured C_p. Normally, the estimation of lattice specific heat is not easy and the Debye formula is often used to approximate it. Fortunately, in our case, data on the isomorphous nonmagnetic compound, CdI_2 are available.[17] In estimating the lattice specific heat of FeI_2, we considered the mass ratio between Fe and Cd.

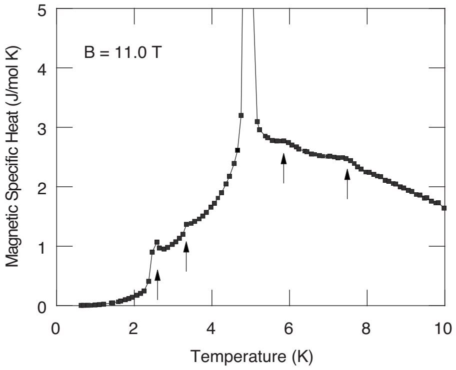

FIG. 7. The temperature dependence of magnetic specific heat in FeI_2 measured at 11.0 T. Five distinct peaks are seen.

In zero field, we see a large anomaly in C_m at $T_N = 9.2 \pm 0.1$ K. This value of T_N is in good agreement with those reported before.[12,18,19] As described in Sec. III, the specific heat was measured with the thermal relaxation method. The relaxation time becomes very long in the vicinity of T_N, reflecting the first-order nature of the phase transition.[18] In Fig. 6, we plot the data which are obtained from the relaxation curve that can be fitted with an exponential function. In finite fields, much smaller anomalies in C_m appear, in addition to the large anomaly at $T_N(B)$. This is understandable since the entropy change associated with the transition from the paramagnetic to ordered phase is much larger than that between ordered phases. To demonstrate the existence of successive phase transitions, we show an example of temperature and field scans in Figs. 7 and 8, respectively.

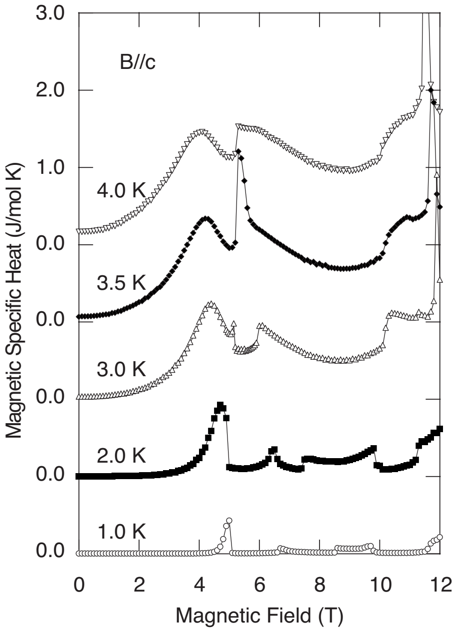

FIG. 8. The magnetic field dependence of magnetic specific heat in FeI_2 measured at representative temperatures. The scale for the ordinate is given to the uppermost curve and the base line for the remaining curves is shifted downwards by 1.0 J/mol K each.

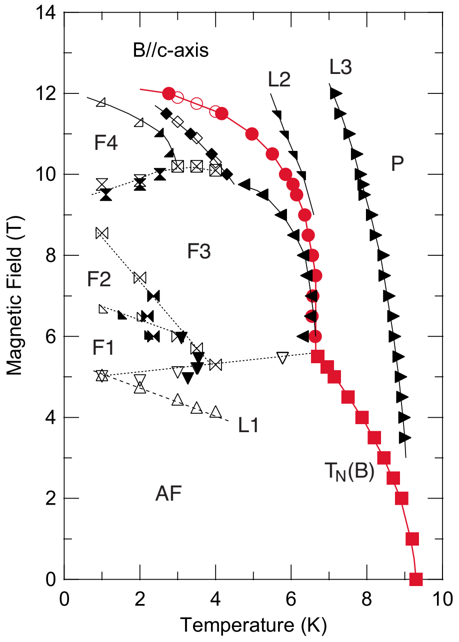

FIG. 9. (Color online) The magnetic field versus temperature phase diagram of FeI_2 determined from the specific-heat measurements. The external magnetic field is applied along the *c* axis of the crystal. Open and filled symbols show, respectively, the transition points found in the field and temperature scans. Red symbols show the transition point at which the largest anomaly in C_m is observed in respective scans. AF: antiferromagnetic phase, P: paramagnetic phase.

Figure 9 shows the temperature versus magnetic field phase diagram constructed from the specific-heat measurements. In this phase diagram we included the data obtained from the temperature and field scans. An overall feature of our phase diagram is consistent with that reported before.[14] New findings in this work are the following. First, we find that phase F3 is magnetically ordered as evidenced by the large anomaly in C_m. Second, we find that phase F4 is divided into three subphases. Third, we find new phase transition lines, L1, L2, and L3.

Because the phase transition lines L2 and L3 are located at the high temperature side above the magnetic phase boundaries, we believe that these represent a structural phase transition. The line L3 seems to merge into the $T_N(B)$ curve with decreasing B. This suggests that the magnetic and structural phase transitions occur simultaneously at $B \simeq 0$. The origin of the phase transition line L1 is not clear at the moment.

V. DISCUSSION

A. Electronic state

The electronic state of an $Fe^{2+}(3d^6)$ ion in a crystal has been studied by several authors.[20–24] The ground state of a free Fe^{2+} ion has total spin $S=2$ and total orbital momentum $L=2$. Under a cubic crystal field, the orbital state splits into a triplet, Γ_5, and a doublet, Γ_3, the former being the ground state.[20] Because the energy difference between the Γ_5 and Γ_3 states is $\sim 10^4$ cm^{-1}, we may consider only the Γ_5 state and use an effective orbital momentum, $\vec{l}(|\vec{l}|=1)$, to discuss the magnetic properties of FeI_2 below room temperature. The effective orbital momentum is related to the original one as, $\vec{L}=-\vec{l}$.[20] The Hamiltonian we consider is given by

$$H = -\lambda \vec{l}\cdot\vec{S} - \delta(l_z^2 - 2/3) + \mu_B \vec{B}\cdot(2\vec{S}-\vec{l}), \qquad (1)$$

where, the first, second, and third terms represent, respectively, the spin-orbit interaction, an additional crystal field with lower symmetry, and the Zeeman effect.

Birgeneau *et al.*[24] derived the energy level scheme of Eq. (1) for $FeCl_2$, in which the ground state is a triplet separated by ~ 100 cm^{-1} from the first excited state. At low temperatures below ~ 140 K(=100 cm^{-1}), one may consider only the ground state and use an effective spin $\vec{s}(|\vec{s}|=1)$. The Hamiltonian describing the $s=1$ multiplet is given by[24]

$$\sum_i D\left[(s_i^z)^2 - \frac{2}{3}\right] + \sum_{i,j}[-2\alpha_\parallel^2 J_{ij} s_i^z s_j^z - 2\alpha_\perp^2 J_{ij}(s_i^x s_j^x + s_i^y s_j^y)], \qquad (2)$$

where, the first and second terms represent, respectively, a single ion anisotropy and an anisotropic exchange interaction with $D=-9.4$ cm^{-1}, $\alpha_\parallel=1.67$, and $\alpha_\perp=1.40$.[24] Because of the strong single ion anisotropy, the states with $s^z=\pm 1$ is highly populated at low temperatures and we may use an Ising spin $\sigma(=\pm 1)$ to discuss the magnetic properties of $FeCl_2$. We expect that essentially the same situation will be realized in FeI_2. The value of D in FeI_2 has been obtained to be -21 K($\simeq -15$ cm^{-1}) from the analysis of the susceptibility data.[12]

B. Exchange interaction

We plot in Fig. 10(a) the transition temperature of FeX_2 compound. Here, X stands for, Cl^-, Br^-, or I^-. The transition temperature decreases rapidly when X changes from Cl, through Br, to I. This suggests that competing interactions, ferromagnetic and antiferromagnetic ones, exist between the Fe spins and the antiferromagnetic interaction becomes strong with X, resulting in the decrease in the transition temperature.

Here, we consider two types of exchange interaction, namely, the direct-exchange and superexchange ones, on a given interaction path. Figure 10(b) shows the bond lengths and bond angle in FeX_2 compound. The bond angle $\angle Fe^{2+}$-X^--Fe^{2+} is almost 90° for the three compounds, $FeCl_2$, $FeBr_2$, and FeI_2. Goodenough[26] argued that the interaction within the layers of the transition element dichlorides and dibromides is the 90° superexchange one and is ferromagnetic if the t_{2g} orbitals are more than half filled. Kanamori[27] showed that the 90° superexchange interaction between $Ni^{2+}(3d^8)$ spins is ferromagnetic. If we accept the above proposition that there are competing ferromagnetic and antiferromagnetic interactions in FeX_2 compound, the direct exchange interaction between Fe spins should be antiferromagnetic. From the magnetic structure mentioned above, we may conclude that the ferromagnetic superexchange interaction dominates in $FeCl_2$ and $FeBr_2$, while the

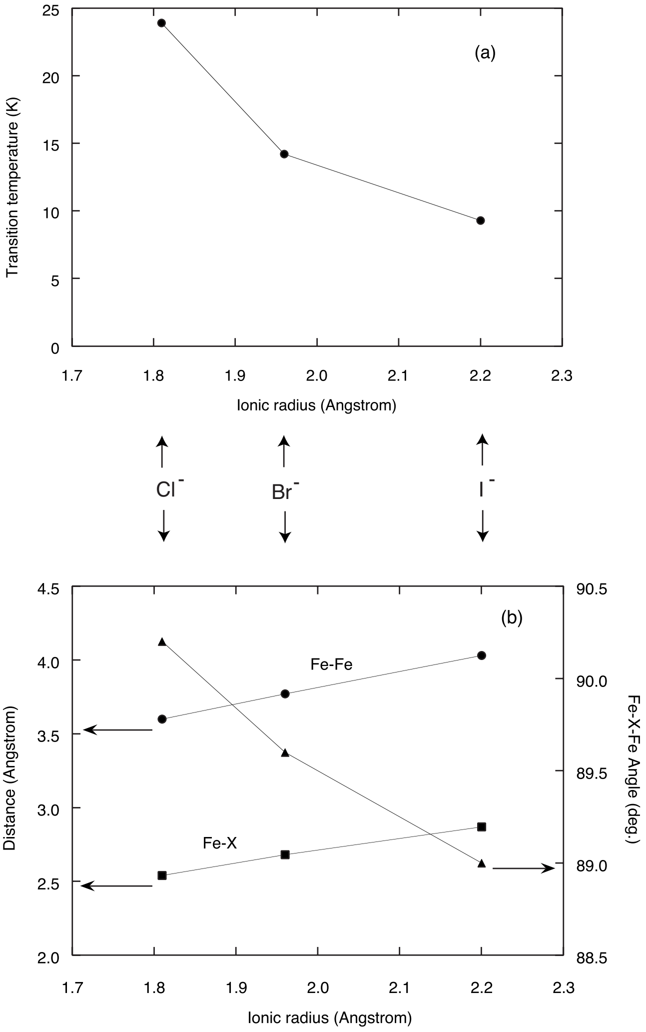

FIG. 10. (a) The transition temperature of FeX_2 (X=Cl, Br, or I) compound is plotted versus the ionic radius of X^- ion. (b) The bond length between Fe^{2+} ions, that between Fe^{2+} and X^- ions and the bond angle $\angle Fe^{2+}$-X^--Fe^{2+} are plotted as a function of the ionic radius (Ref. 25).

antiferromagnetic direct-exchange interaction plays a dominant role in FeI_2. Based on this idea and the experimental fact shown in Fig. 10(b), we may conclude that the antiferromagnetic interaction in FeX_2 compound becomes strong with the distance, $d_{\text{Fe-Fe}}$, between Fe spins.

Zener[28] argued that the exchange integral between d shells of adjacent atoms has always the same sign as in the H_2 molecule. The exchange potential in the H_2 molecule giving rise to the spin singlet state is negative (antiferromagnetic) at the interatomic distances larger than a_0 and has a minimum at $\frac{3}{2}a_0$, where a_0 is the Bohr radius.[29] The experimental finding that the antiferromagnetic interaction in FeX_2 compound becomes stronger with increasing $d_{\text{Fe-Fe}}$ suggests $d_{\text{Fe-Fe}}$ is shorter than the distance where the exchange potential is at a minimum.

C. Phase transition in zero field

The magnetic ordering in FeI_2 has been discussed in terms of the further neighbor interaction model on the triangular net.[12,14] However, the exchange interaction constants derived from these studies do not seem to be realistic. We discuss the phase transition based on the anisotropic triangular lattice model. In order to be consistent with this model, a lattice distortion should take place at T_N. In fact, a lattice distortion has been observed at the lower transition temperature, T_{N2} of a triangular lattice antiferromagnet, $CuFeO_2$ in zero field.[30] When an external magnetic field is applied, the lattice constant of $CuFeO_2$ is seen to change stepwise in coincidence with the multistep magnetization changes.[31,32] An evidence of a magnetoelastic coupling in FeI_2 has been found from a neutron-diffraction study, where the transition at T_N is seen to be of first order.[18] As explained in Sec. IV C, our specific-heat measurements suggest that the magnetic order and structural change occur simultaneously at T_N.

The magnetic structure predicted from the anisotropic triangular lattice model is shown in Fig. 1(c), which is different from the magnetic structure in the c plane of FeI_2 determined experimentally [Fig. 2(b)]. In the following discussion, we consider the case in which the exchange interaction constant for parallel spins may be different from that for antiparallel spins. This comes from the nature of the exchange interaction discussed above. The distance between parallel spins of a given exchange bond may be shorter than that between antiparallel spins to diminish the antiferromagnetic direct-exchange energy. Writing an exchange interaction between Ising spins, σ_i and $\sigma_j(\sigma=\pm 1)$ as

$$-\Sigma_{i,j}J_{i,j}\sigma_i\sigma_j, \tag{3}$$

the energy, E_{AF}, of the antiferromagnetic state of FeI_2 is given by

$$E_{\text{AF}}/N = \frac{1}{2}(2J_1 + J_2 - J_2' + J_3 - J_3'), \tag{4}$$

where, J_k' (k=1, 2, and 3) is the exchange interaction constant between parallel spins along the J_k bond and N is the number of spins in the sample. The energy, E_{Stephen}, of the magnetic structure shown in Fig. 1(c) is given by

$$E_{\text{Stephen}}/N = J_1 + J_2 - J_3'. \tag{5}$$

The condition that E_{AF} is lower than E_{Stephen} is given by

$$0 < J_2 + J_2' - J_3 - J_3'. \tag{6}$$

D. Magnetization

1. High field magnetization

As described in Sec. IV B, the magnetization of FeI_2 increases steadily with increasing field. This suggests a contribution of the higher energy crystal-field levels. We calculate rigorously the 15 eigenvalues of Eq. (1) using the MATHEMATICA.[33] Then, the magnetization is calculated with a standard procedure of statistical mechanics using the MATHEMATICA. We are able to reproduce qualitatively the experimental finding that the magnetization increases steadily with increasing field.

Here, we have two free parameters, λ and δ, to fit the theory with the experiment. Different values of λ and δ have been reported by different authors; $\lambda=-95$ cm^{-1} and $\delta=119$ cm^{-1} in FeCl$_2$,[21] $\lambda=-67$ cm^{-1} and $\delta=88$ cm^{-1} in FeCl$_2$,[23,24] and $\lambda=-73$ cm^{-1} and $\delta=183$ cm^{-1} in FeI$_2$.[22] The set of λ and δ values reported by Ôno *et al.*[21] is the closest to the measurement but none of these parameter sets reproduce quantitatively the experimental result. For a quantitative analysis of the magnetization curve, the exchange interaction should be taken into account.

2. Magnetization process

We try to extract an intrinsic magnetization curve of FeI$_2$ from the measured ones. We have shown that the higher energy crystal-field levels give a magnetization that increases steadily with increasing field. This might give the initial slope in the magnetization curve shown in Fig. 4. From a fit of the magnetization curve calculated in Sec. V D 1 to a linear function in B, we obtain the susceptibility, $\chi_{\text{cf}}=0.004$ (emu/mole), due to the crystal-field levels when $\lambda=-95$ cm^{-1} and $\delta=119$ cm^{-1}. This value of χ_{cf} is considerably smaller than $\chi_{\parallel}(T\to 0)\simeq 0.055$ (emu/mole) or $\chi_{\parallel}(T\to 0)\simeq 0.017$ (emu/mole) reported in Sec. IV A.

As is seen in Fig. 4, the two magnetization curves measured on the samples #1 and 2 become almost identical above ~10 T. This means that the impurity spins on the crystal imperfections are not free. Instead, an interaction exists among the impurity spins, the strength of which is sample dependent. We assume a generalized Brillouin function given by Eq. (7) to describe the magnetization, M_{imp}, due to the impurities, in units of μ_{B}/ion,

$$M_{\text{imp}} = \alpha g S[\{(2S+1)/(2S)\}\coth\{(2S+1)y/(2S)\} - \{1/(2S)\}\coth\{y/(2S)\}], \quad (7)$$

where, $y\equiv \beta g S \mu_{\text{B}} B/(k_{\text{B}}T)$, μ_{B} the Bohr magneton, k_{B} the Boltzmann constant, α the fraction of the impurities, and β represents an interaction between the impurity spins. We use $g=3.5$ obtained from the ESR measurements[15,16] and $S=2$ which is widely accepted for an Fe^{2+} ion. The values of α and β are determined so that the two magnetization curves measured on the samples #1 and 2 become as close as possible. We subtracted the $\chi_{\text{cf}}\cdot B$ term discussed above from the measured magnetization curves before applying Eq. (7). The intrinsic magnetization curves thus obtained are shown in Fig. 11. A reasonably good agreement between the two magnetization curves is obtained with $\alpha=0.055$ and $\beta=0.24$, and $\alpha=0.088$ and $\beta=0.049$, for the samples #1 and 2, respectively.

We see in Fig. 11 that the magnetization steps are located at, $\frac{1}{3}M_{\text{s}}$, $\frac{12}{25}M_{\text{s}}$, $\frac{13}{25}M_{\text{s}}$ and between $\frac{16}{25}M_{\text{s}}$ and $\frac{17}{25}M_{\text{s}}$. For the value of M_{s}, we use 3.5 μ_{B}/Fe, which is given by $g\cdot\sigma$ (see Sec. IV B). From the pulsed field measurement, we have obtained $M_{\text{s}}\simeq 3.8$ μ_{B}/Fe, which becomes $M_{\text{s}}\simeq 3.7$ μ_{B}/Fe, after subtracting the $\chi_{\text{cf}}\cdot B$ term. A further subtraction of the magnetization due to the impurities will give a value close to 3.5 μ_{B}/Fe.

Wiedenmann *et al.*[14] have reported the observation of magnetization steps at, $0.33M_{\text{s}}$, $0.45M_{\text{s}}$, $0.5M_{\text{s}}$, and $0.6M_{\text{s}}$ with $M_{\text{s}}=4.1$ μ_{B}/Fe. Our observation of the $\frac{1}{3}M_{\text{s}}$ step is consistent with that by Wiedenmann *et al.* However, the $\frac{12}{25}=0.48$, $\frac{13}{25}=0.52$, $\frac{16}{25}=0.64$, and $\frac{17}{25}=0.68$ steps are not reproduced. The reason for this discrepancy is that Wiedenmann *et al.* subtracted a magnetization that increases linearly in B from the measured magnetization. The origin of this linear magnetization has not been discussed.

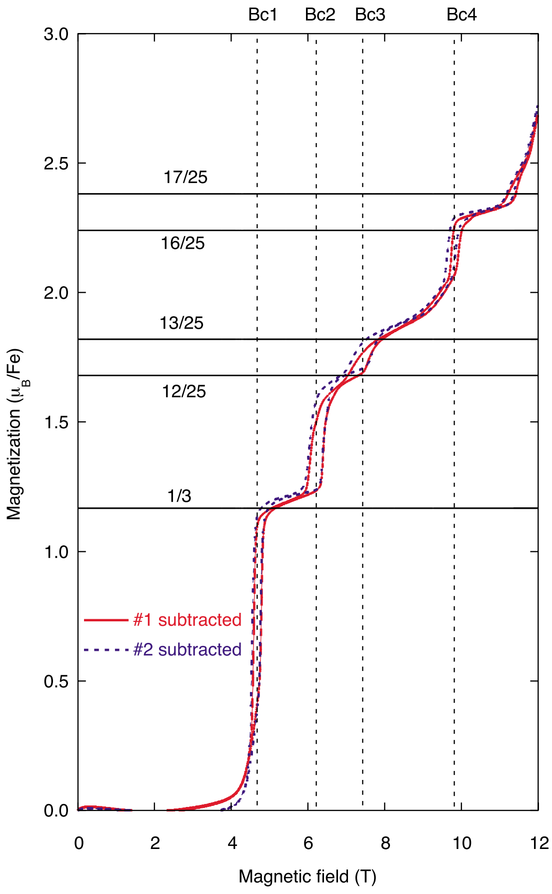

FIG. 11. (Color online) The magnetization curve of FeI$_2$ after subtracting the contribution of impurities and crystal-field levels.

We propose a possible magnetic structure for each of the $\frac{12}{25}M_{\text{s}}$, $\frac{13}{25}M_{\text{s}}$, $\frac{16}{25}M_{\text{s}}$, and $\frac{17}{25}M_{\text{s}}$ phases. The magnetic structure of the $\frac{1}{3}M_{\text{s}}$ phase is given in Fig. 3(b). The experimental fact obtained from the neutron diffraction[14] is that the wave vector $\boldsymbol{k}=[\frac{1}{5}\frac{1}{5}0]$ is observed in phases F2 and F4. We have observed a magnetic long-range order in phase F3 from our neutron-diffraction experiment with the wave vector $\boldsymbol{k}=[h,h,0]$, where, $h\simeq\frac{1}{5}$.[34] These facts mean that the magnetic unit cell in the c plane of phases F2, F3, and F4 is a $5a\times 5a$ one. If we assume up or down states only for each of the magnetic moment in the unit cell, we expect the magnetization steps to appear at $\frac{9}{25}M_{\text{s}}$, $\frac{11}{25}M_{\text{s}}$, $\frac{13}{25}M_{\text{s}}$, $\frac{15}{25}M_{\text{s}}$, $\frac{17}{25}M_{\text{s}}$, $\frac{19}{25}M_{\text{s}}$, $\frac{21}{25}M_{\text{s}}$, and $\frac{23}{25}M_{\text{s}}$. Here, we have considered the states with the magnetization larger than $\frac{1}{3}M_{\text{s}}$. From this consideration, the magnetization steps at $\frac{12}{25}M_{\text{s}}$ and $\frac{16}{25}M_{\text{s}}$ are not explained. Then, we allow some of the down spins to take $\langle\sigma\rangle=-\frac{1}{2}$ value. Figure 12 shows the proposed magnetic structure for each of the $\frac{12}{25}M_{\text{s}}$ and $\frac{16}{25}M_{\text{s}}$ phases. The magnetic structure with $\frac{13}{25}M_{\text{s}}$ is obtained by reversing six spins from a fully saturated state. Since this magnetic structure is less symmetric, we propose the structure shown in Fig. 12, in

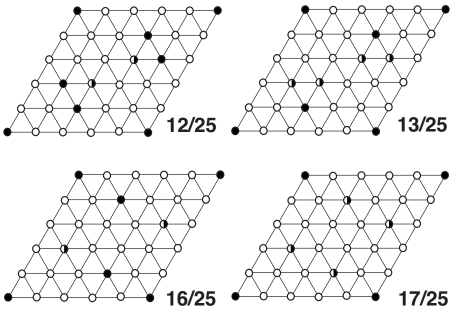

FIG. 12. A possible magnetic structure for the $\frac{12}{25}M_{\rm s}$, $\frac{13}{25}M_{\rm s}$, $\frac{16}{25}M_{\rm s}$, and $\frac{17}{25}M_{\rm s}$ states, respectively. Open, filled, and half-filled circles represent, respectively, up, down, and $\langle\sigma\rangle=-\frac{1}{2}$ moments.

which the four down spins have $\langle\sigma\rangle=-\frac{1}{2}$ value. We propose the magnetic structure for the $\frac{17}{25}M_{\rm s}$ phase shown in Fig. 12 from the same reason mentioned above.

In the following, we calculate the transition fields between the different phases, from which we try to deduce the exchange interaction constants. Because the measurement of the magnetization curve is made at the low temperature well below $T_{\rm N}$, we may calculate the energy of each phase at $T=0$ based on the Hamiltonian, Eq. (3). Although the $\langle\sigma\rangle=-\frac{1}{2}$ value is expected to appear at a finite temperature, we assume, for simplicity, $\sigma=-\frac{1}{2}$ for the magnetic moment at the half-filled cites in Fig. 12.

The energy, $E_{\rm AF}$, of the antiferromagnetic phase is given by Eq. (4). The energy, $E_{1/3}$, of the $M_{\rm s}/3$ phase is given by

$$E_{1/3}/N=\frac{1}{6}(2J_1-4J_1'+3J_2-3J_2'+2J_3-4J_3'-2g\mu_{\rm B}B). \tag{8}$$

The energy, $E_{12/25}$, of the $12M_{\rm s}/25$ phase is given by

$$E_{12/25}/N=\frac{1}{25}(8J_1-13J_1'+J_1''-J_1'''+6J_2-15J_2'+2J_2''+8J_3-13J_3'+J_3''-J_3'''-12g\mu_{\rm B}B), \tag{9}$$

where, $J_{1,2,3}''$ is the exchange interaction constant between the up and $\sigma=-\frac{1}{2}$ spins, and $J_{1,2,3}'''$ is that between the down and $\sigma=-\frac{1}{2}$ spins.

The energy, $E_{13/25}$, in the $13M_{\rm s}/25$ phase is given by

$$E_{13/25}/N=\frac{1}{25}(6J_1-13J_1'+2J_1''-J_1''''/2+4J_2-13J_2'+3J_2''-J_2'''+4J_3-13J_3'+4J_3''-J_3'''-13g\mu_{\rm B}B), \tag{10}$$

where, $J_{1,2,3}''''$ is the exchange interaction constant between the $\sigma=-\frac{1}{2}$ spins.

The energy, $E_{16/25}$ in the $16M_{\rm s}/25$ phase is given as

$$E_{16/25}/N=\frac{1}{25}(6J_1-15J_1'+2J_1''+6J_2-15J_2'+2J_2''+6J_3-15J_3'+2J_3''-16g\mu_{\rm B}B). \tag{11}$$

The energy, $E_{17/25}$ in the $17M_{\rm s}/25$ phase is given by

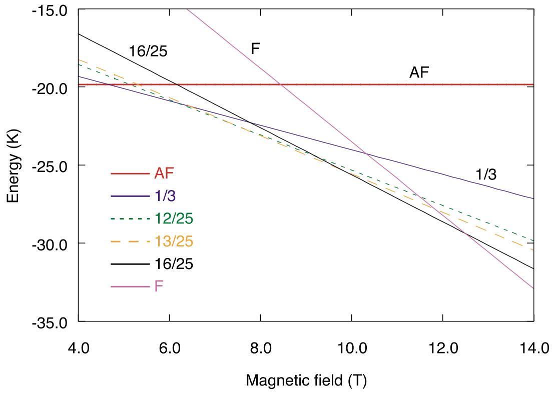

FIG. 13. (Color online) The magnetic field dependence of the energy in the AF, $M_{\rm s}/3$, $12M_{\rm s}/25$, $13M_{\rm s}/25$, $16M_{\rm s}/25$ and saturated F phases, respectively. The energy is measured from that of the saturated ferromagnetic phase.

$$E_{17/25}/N=\frac{1}{25}(2J_1-15J_1'+4J_1''+2J_2-15J_2'+4J_2''+2J_3-15J_3'+4J_3''-17g\mu_{\rm B}B). \tag{12}$$

Finally, the energy, $E_{\rm F}$, of the saturated ferromagnetic phase is expressed as

$$E_{\rm F}/N=(-J_1'-J_2'-J_3'-g\mu_{\rm B}B). \tag{13}$$

We define the critical fields, $B_{{\rm c}i}$ ($i=1$, 2, 3, and 4), as shown in Fig. 11. The critical field, $B_{\rm c5}$ is defined as the one at which the transition to the saturated ferromagnetic phase occurs. The critical field, $B_{\rm c1}$, is given by the field at which $E_{\rm AF}$ and $E_{1/3}$ become equal. Other critical fields are given similarly. The value of the critical fields obtained experimentally is, $B_{\rm c1}=4.67\pm0.05$ T, $B_{\rm c2}=6.22\pm0.05$ T, $B_{\rm c3}=7.43\pm0.05$ T, and $B_{\rm c4}=9.82\pm0.05$ T. Here we take an average of the critical fields obtained in the increasing and decreasing fields as shown in Fig. 11. For the value of $B_{\rm c5}$ we take 12.5 ± 0.1 T obtained from the pulsed field measurement.

Figure 13 shows the magnetic field dependence of $E_{\rm AF}$, $E_{1/3}$, $E_{12/25}$, $E_{13/25}$, $E_{16/25}$, and $E_{\rm F}$. A similar diagram is obtained when we take the $E_{17/25}$ phase, instead of the $E_{16/25}$ one. The value of these energies at zero field measured from $E_{\rm F}$ is

$$E_{\rm AF}(B=0)/k_{\rm B}=-19.9\ \ {\rm K},$$

$$E_{1/3}(B=0)/k_{\rm B}=-16.2\ \ {\rm K},$$

$$E_{12/25}(B=0)/k_{\rm B}=-14.0\ \ {\rm K},$$

$$E_{13/25}(B=0)/k_{\rm B}=-13.3\ \ {\rm K},$$

$$E_{16/25}(B=0)/k_{\rm B}=-10.6\ \ {\rm K}. \tag{14}$$

The saturated ferromagnetic phase is indistinguishable from the paramagnetic phase above $T_{\rm N}$, where no lattice distortion is assumed. Therefore, we may set, $J_1'=J_2'=J_3'\equiv J'$ in Eq. (13). We assume $J_1'=J_2'=J_3'$ at all fields below $B_{\rm c5}$. Using the value of $\Theta/k_B = -21.5$ K,[12] we have $J'/k_B = -3.58$ K, where Θ is the Curie temperature. Then, the energy, $E_F(B=0)/k_B$, of the F phase in zero field is estimated as 10.7 K. Thus, all the energies in respective phases at $B=0$ are determined in units of kelvin.

We determine the value of the exchange interaction constants by solving the simultaneous equations, Eqs. (4), (8)–(11), and (13). Because the number of exchange interaction constants is larger than the experimental data available, we have to reduce it. We assume, $J_i'' \simeq J_i$, $J_i''' \simeq J_i'$, and $J_i'''' \simeq J_i'$, where, $i=1$, 2, and 3. From the calculation we have

$$2.5 < J_1/k_B < 3.0 \text{ K},$$

$$-16.2 < J_2/k_B < -15.2 \text{ K},$$

$$-16.4 < J_3/k_B < -14.4 \text{ K}. \quad (15)$$

If we choose the $17M_s/25$ phase, instead of the $16M_s/25$ one, we obtain,

$$2.5 < J_1/k_B < 3.0 \text{ K},$$

$$-15.7 < J_2/k_B < -14.7 \text{ K},$$

$$-16.1 < J_3/k_B < -14.3 \text{ K}. \quad (16)$$

We see that the exchange interaction J_1 is ferromagnetic while J_2 and J_3 are antiferromagnetic. From the discussion given in Sec. V B, we predict that $d_{\text{Fe-Fe}}$ along the J_1 interaction path shrinks below T_N. We note that Petitgrand *et al.*[35] showed that the nearest-neighbor exchange interaction is ferromagnetic and the next-nearest-neighbor one is antiferromagnetic from the far-infrared absorption measurement on FeI_2.

VI. CONCLUSIONS

We have measured the magnetic susceptibility, magnetization, and specific heat on the single crystals of FeI_2 grown by ourselves. From the specific-heat measurement, we have constructed the temperature versus magnetic field phase diagram, in which five distinct magnetic phases, namely, the antiferromagnetic and four ferrimagnetic ones (F1, F2, F3, and F4) exist. The magnetization measurement reveals that magnetization steps appear at $\frac{1}{3}$, $\frac{12}{25}$, $\frac{13}{25}$ and between $\frac{16}{25}$ and $\frac{17}{25}$ of the saturation magnetization, $M_s = 3.5\ \mu_B/\text{Fe}$.

We discussed the ground state and exchange interaction in FeI_2 and justified that the material is modeled as an Ising antiferromagnet on the triangular lattice, to a good approximation. We proposed that there are two competing exchange interactions in the MX_2 compound, namely, an antiferromagnetic direct-exchange and ferromagnetic superexchange ones and that the former interaction dominates in FeI_2. Based on an experimental evidence, we argued that a lattice distortion occurs below T_N and the exchange interaction between spins on a triangle becomes anisotropic. We analyzed the phase transition based on the anisotropic triangular lattice model with J_1, J_2, and J_3. From the analysis of the metamagnetic transition fields, we obtain, $2.5 < J_1/k_B < 3.0$ K, $-16.2 < J_2/k_B < -15.2$ K, and $-16.4 < J_3/k_B < -14.4$ K. We predicted that $d_{\text{Fe-Fe}}$ along the J_1 interaction path shrinks below T_N. An x-ray diffraction study on this sample below T_N would be valuable to test this prediction, provided that a crystal of high quality is available.

ACKNOWLEDGMENTS

We would like to thank S. Sasaki for helpful discussions. This work was supported in part by the Grant-in-Aid for Scientific Research on priority Areas "High Field Spin Science in 100 T" (Grant No. 451) from the Ministry of Education, Culture, Sports, Science and Technology (MEXT).

---

[1] G. H. Wannier, Phys. Rev. **79**, 357 (1950); Phys. Rev. B **7**, 5017 (1973).

[2] C. Domb, Adv. Phys. **9**, 149 (1960).

[3] B. D. Metcalf, Phys. Lett. A **45**, 1 (1973).

[4] J. Stephenson, J. Math. Phys. **11**, 420 (1970).

[5] J. Kanamori, Prog. Theor. Phys. **35**, 16 (1966).

[6] B. D. Metcalf, Phys. Lett. A **46**, 325 (1974).

[7] Y. Tanaka and N. Uryû, Prog. Theor. Phys. **55**, 1356 (1976).

[8] M. Kaburagi, T. Tonegawa, and J. Kanamori, J. Phys. Soc. Jpn. **53**, 1971 (1984).

[9] For a review see, K. Katsumata, *Landolt-Börnstein*, New Series, Group III, Vol. 27j1, edited by H. P. J. Wijn (Springer-Verlag, Berlin, 1994), p. 1, and references therein.

[10] M. K. Wilkinson, J. W. Cable, E. O. Wollan, and W. C. Koehler, Phys. Rev. **113**, 497 (1959).

[11] J. Gelard, A. R. Fert, P. Meriel, and Y. Allain, Solid State Commun. **14**, 187 (1974).

[12] Y. Bertrand, A. R. Fert, and J. Gélard, J. Phys. (France) **35**, 385 (1974).

[13] A. R. Fert, J. Gelard, and P. Carrara, Solid State Commun. **13**, 1219 (1973).

[14] A. Wiedenmann, L. P. Regnault, P. Burlet, and J. Rossat-Mignod, J. Magn. Magn. Mater. **74**, 7 (1988).

[15] A. R. Fert, D. Bertrand, J. Leotin, J. C. Ousset, J. Magariño, and J. Tuchendler, Solid State Commun. **26**, 693 (1978).

[16] K. Katsumata, H. Yamaguchi, M. Hagiwara, M. Tokunaga, H.-J. Mikeska, P. Goy, and M. Gross, Phys. Rev. B **61**, 11632 (2000).

[17] E. S. Itskevich and P. G. Strelkov, Sov. Phys. JETP **5**, 394 (1957).

[18] D. Petitgrand, B. Hennion, and C. Escribe, J. Phys. (France) **41**, L-135 (1980).

[19] R. M. Brade and B. Yates, J. Phys. C **4**, 876 (1971).

[20] J. Kanamori, Prog. Theor. Phys. **17**, 177 (1957).

[21] K. Ôno, A. Ito, and T. Fujita, J. Phys. Soc. Jpn. **19**, 2119 (1964).

[22] T. Fujita, A. Ito, and K. Ôno, J. Phys. Soc. Jpn. **21**, 1734 (1966).

[23] R. Alben, J. Phys. Soc. Jpn. **26**, 261 (1969).

[24] R. J. Birgeneau, W. B. Yelon, E. Cohen, and J. Makovsky, Phys. Rev. B **5**, 2607 (1972).

[25] Calculated with the CRYSTALMAKER manufactured by the CrystalMaker Software Ltd., Centre for Innovation & Enterprise, Begbroke Science Park, Oxford, OX5 1PF, UK.

[26] J. B. Goodenough, *Magnetism and the Chemical Bond* (Interscience, New York, 1963).

[27] J. Kanamori, J. Phys. Chem. Solids **10**, 87 (1959).

[28] C. Zener, Phys. Rev. **81**, 440 (1951).

[29] W. Heitler and F. London, Z. Phys. **44**, 455 (1927).

[30] N. Terada, S. Mitsuda, H. Ohsumi, and K. Tajima, J. Phys. Soc. Jpn. **75**, 023602 (2006).

[31] N. Terada, Y. Narumi, K. Katsumata, T. Yamamoto, U. Staub, K. Kindo, M. Hagiwara, Y. Tanaka, A. Kikkawa, H. Toyokawa, T. Fukui, R. Kanmuri, T. Ishikawa, and H. Kitamura, Phys. Rev. B **74**, 180404(R) (2006).

[32] N. Terada, Y. Narumi, Y. Sawai, K. Katsumata, U. Staub, Y. Tanaka, A. Kikkawa, T. Fukui, K. Kindo, T. Yamamoto, R. Kanmuri, M. Hagiwara, H. Toyokawa, T. Ishikawa, and H. Kitamura, Phys. Rev. B **75**, 224411 (2007).

[33] Software manufactured by the Wolfram Research, Inc., 100 Trade Center Drive, Champaign, IL 61820-7237, USA.

[34] K. Katsumata, H. A. Katori, and K. Prokes, *BENSC Experimental Reports* (Helmholtz-Zentrum Berlin, Berlin, 2001).

[35] D. Petitgrand, A. Brun, and P. Meyer, J. Magn. Magn. Mater. **15-18**, 381 (1980).